PAPER

The enhanced magnetorheological performance of carbonyl iron suspensions using magnetic Fe₃O₄/ZHS hybrid composite sheets

Michal Machovský,[a] Miroslav Mrlík,*[ab] Tomáš Plachý,[ac] Ivo Kuřitka,[a] Vladimír Pavlínek,[a] Zuzana Kožáková[a] and Takeshi Kitano[a]

Two-dimensional magnetic Fe₃O₄/ZHS hybrid composite sheets were prepared *via* a two-step microwave-assisted solvothermal synthesis. The successful incorporation of Fe₃O₄ nanoparticles synthesized in the first step into a zinc hydroxysulfate (ZHS) sheet-like structure formed during the second synthesis step was confirmed by X-ray diffraction, scanning electron microscopy, and vibrating sample magnetometry. The obtained magnetic Fe₃O₄/ZHS hybrid composite particles show a hexagonal and sheet-like morphology. The addition of these sheet-like hybrid composite particles into magnetorheological carbonyl iron-based suspensions results in a significant increase in MR performance. Moreover, this addition considerably contributes to the redispersibility enhancement of prepared suspensions in comparison to those consisting only of bare carbonyl iron particles.

1. Introduction

Magnetorheological (MR) suspensions are smart materials, the rheological properties of which exhibit a transition from a liquid-like to solid-like state reversibly after exposure to an external magnetic field.[1–3] Such suspensions are usually composed of micron-sized ferromagnetic[4–6] particles with high saturation magnetization dispersed in a nonmagnetic carrier liquid. However, ferrimagnetic particles with considerably lower values of magnetization have also been successfully applied.[7,8] Generally, in the absence of an external magnetic field, the particles are randomly dispersed in the carrier liquid and the suspensions exhibit a Newtonian-like behaviour. After the application of the external magnetic field, particles are magnetized, which due to the induced magnetic dipoles, results in the formation of chain-like internal structures in the direction of the magnetic field streamlines. Such internal structures restrict the flow, and the suspension becomes pseudoplastic, exhibiting yield stress. In this case, the basic rheological properties such as viscosity and viscoelastic moduli can increase by several orders of magnitude.[9–14]

Therefore, due to their extraordinary properties, MR suspensions have recently begun to be utilized in many industrial applications. These materials provide a rapid response to the magnetic field, and thus they were successfully applied as electronic controls and mechanical systems, which include rotary brakes, dampers, clutches, shock absorbers and torque transducers.[15–17] Besides the established commercial use of MR fluids in the automotive industry, developments might also be expected in the field of medicine, as artificial muscles or for local embolization of blood vessels.[18,19]

Although these materials have advantages, there are still some disadvantages limiting their broad employment. Along with poor stability properties such as chemical[20] and thermo-oxidation,[21] sedimentation along with redispersibility are the crucial factors influencing their lack of effectivity in real-life applications. Many research groups have concentrated on solving these problems by various approaches, *i.e.*, using thixotropic agents and surfactants,[22] or utilizing the core–shell composite particles based on an inorganic-polymer,[23–25] inorganic-MWCNT,[26–28] inorganic–inorganic[29,30] or inorganic-low molecular weight substance[31,32] and finally by employing extremely bidispersed particle mixtures based on CI and magnetite nanoparticles,[33] or dimorphic CI and Fe rod-like particles.[34] Moreover, recently it was determined that MR performance can be enhanced by a small addition of magnetic particles usually in nanoscale order,[35] but also by the addition of non-magnetic ones,[36] which also successfully negate the crucial disadvantages.

Therefore, in this study a rapid microwave-assisted synthesis was utilized to prepare the micro-sized particles of magnetite/zinc hydroxysulfate (Fe₃O₄/ZHS) hybrid composite sheets as an additive for MR suspensions. The successful synthesis was confirmed by X-ray diffraction and SEM analyses. The magnetic characteristics of the additive as well as CI particles were evaluated using vibrating sample magnetometry (VSM). The

[a]Centre of Polymer Systems, University Institute, Tomas Bata University in Zlin, Nad Ovcirnou 3685, 760 01 Zlin, Czech Republic. E-mail: mrlik@ft.utb.cz

[b]Centre for Advanced Materials, Qatar University, P. O. BOX 2713, Doha, Qatar

[c]Polymer Centre, Faculty of Technology, Tomas Bata University in Zlin, nam. TGM 275, 762 72 Zlin, Czech Republic

improved rheological properties in the absence and in the presence of the external magnetic field of the suspensions containing a synthesized additive were reported, and the influence of the additive content on the final MR performance was investigated as well. The contribution of the novel MR suspension composition to the stability properties was evaluated by means of redispersibility measurements.

2. Experimental

2.1 Materials

Iron(III) chloride hexahydrate $FeCl_3 \cdot 6H_2O$, ethylene glycol, ammonium bicarbonate NH_4HCO_3, zinc sulphate monohydrate $ZnSO_4 \cdot H_2O$ and hexamethylenetetramine $(CH_2)_6N_4$ were all purchased from PENTA (Czech Republic), and used as received without further purification. Demineralized water was used throughout the experiments. Carbonyl iron microparticles (SL grade) consisting of >97% of iron particles produced by BASF (Germany) was also utilized.

2.2 Synthesis of Fe_3O_4/ZHS hybrid composite sheets

Fe_3O_4/ZHS hybrid composite sheets were fabricated in two steps *via* microwave-assisted solvo-thermal synthesis. In the first step, magnetic nanoparticles were prepared according to our previous work with slightly modified procedure[37] as follows: NH_4HCO_3 (50 mmol) was added to a solution of $FeCl_3 \cdot 6H_2O$ (5 mmol) in ethylene glycol (60 mL) and heated at 220 °C in a microwave oven for 60 minutes. After cooling to room temperature, the black precipitate was collected by the use of a permanent magnet and washed with water several times.

In the second step, based on our previous work describing the preparation of the pure ZHS sheets,[38] the novel approach was developed to prepare magnetic hybrid composite sheets (Fig. 1). Magnetic nanoparticles were sonicated in 100 mL of aqueous solution containing 3 mmol of $ZnSO_4 \cdot H_2O$ for 5 minutes. After that, 3 mmol of $(CH_2)_6N_4$ dissolved in 50 mL of water were added and the obtained suspension was exposed to microwave irradiation for 10 minutes. After cooling the system, particles were collected by filtration, washed thoroughly with water and dried. The whole procedure was performed three times with different initial amounts of 50, 100, and 150 mg of magnetic nanoparticles, and obtained samples were denoted as S1, S2 and S3, respectively. Dried filtration cakes were always gently crushed into fine powders, which were collected with a permanent magnet. This observation serves as initial evidence for the successful preparation of magnetic Fe_3O_4/ZHS nanocomposites. ZHS reference material was prepared without the addition of magnetic nanoparticles, keeping other parameters of the synthesis the same.

2.3 Characterization

Crystalline phases of powder samples were characterized by the powder X-ray diffractometer X'Pert PRO X-ray (PANalytical, The Netherlands) with a Cu-K_α X-ray source ($\lambda = 1.5418$ Å) in the diffraction angle range of $2\theta = 5-85°$. The morphology and structure were observed by the scanning electron microscope
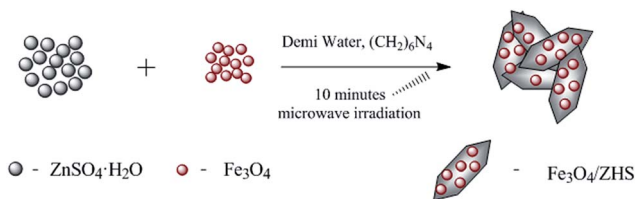

Fig. 1 Schematic illustration of Fe_3O_4/ZHS hybrid composite sheets synthesis procedure.

Vega II/LMU (Tescan, Czech Republic) operated at 10 kV. The magnetic properties were studied using a vibrating sample magnetometer VSM 7400 (Lake Shore, United States).

2.4 Suspension preparation

Bare CI particles were suspended in silicone oil (Lukosiol M 200, viscosity $\eta_c = 194$ mPa s, density $d_c = 0.970$ g cm^{-3}, relative permittivity $\varepsilon' = 2.89$, loss factor tan $\delta = 0.0001$, Chemical Works Kolín, Czech Republic) at fixed 80 wt% particle concentrations. Furthermore, in order to evaluate the impact of the hybrid composite sheets on the MR performance, two different amounts were used (1 wt% and 5 wt%). For this purpose sample S3, due to its suitable magnetic properties, was used. Then the suspensions were mechanically stirred and sonicated for 30 s before each measurement.

2.5 Redispersibility measurements

Redispersibility measurements were performed according to the ASTM-D5-05a standard method, when the standard needle penetrates the suspension with a fixed velocity 10 mm s^{-1} and the stiffness is recorded by an analytical balance (ABJ 120-4 KERN, Germany) with 0.1 mg accuracy. A similar procedure was also successfully applied by another research group.[39]

2.6 Rheological properties

The rheological properties under an external magnetic field in the range 0–300 mT were investigated using a rotational rheometer Physica MCR 502 (Anton Paar GmbH, Austria) equipped with a Physica MRD 170/1T magneto-cell. The geometry gap was set to 0.5 mm. The investigation under steady state conditions were performed in range from 0.1 up to 300 s^{-1} and 5 points per decade were recorded. Each point was calculated without certain time limitation, thus necessary time to reach equilibrium state for calculation of each point was provided. The true magnetic flux density was measured using a Hall probe, and the temperature was controlled by an external thermostat (Julabo, Germany). All rheological experiments were performed at a temperature of 25 °C.

2.7 Microscopic observation

Suspensions consisting of 20 wt% of bare CI particles, with 20 wt% and corresponding amounts of magnetic additive S3 (in order to obtain same ratio between the CI and S3 similarly as was used for rheological experiments) in silicone oil were placed

between two magnet plates with a gap of 0.5 mm providing the magnetic flux density of 120 mT. The formation of MR structures was observed with the help of an optical microscope (N 400M, China) linked to a digital camera.

3.   Results and discussion

3.1   Structure characterization and magnetic properties

The XRD patterns of Fe_3O_4/ZHS hybrid composite sheets prepared at different loading levels of Fe_3O_4 and reference raw materials are shown in Fig. 2. The XRD patterns of Fe_3O_4 show main peaks at $2\theta = 30.1°$, $35.5°$, $43.2°$, $53.6°$, $57.1°$, $62.7°$ and $74.2°$ (indicated by stars) corresponding to (220), (311), (400), (422), (511), (440) and (533) Bragg reflections, respectively. Positions of peaks can be assigned either to magnetite ($Fe(II)Fe(III)_2O_4$) (ICDD-JCPDS PDF-2 entry 01-072-130500-007-0322) or maghemite (γ-$Fe(III)_2O_3$) (ICDD-JCPDS PDF-2 entry 01-072-1305 00-004-0755). As both phases possess the same spinel structure and thus have almost identical lattice parameters, precise identification is quite difficult and highly sophisticated equipments and techniques are usually required, although a method based solely on high resolution XRD analysis has been recently proposed.[9] Regardless of this well-known ambiguity, the preparation of highly crystalline ferrite spinel nanoparticles was confirmed.

Powder XRD patterns of ZHS reference exhibit sharp reflections in the range of small Bragg angles and broad and asymmetric reflections in the range of high angles as typical for layered structures.[10] Here, a series of peaks correspond to zinc sulphate hydroxide tetrahydrate $Zn_4SO_4(OH)_6 \cdot 4H_2O$ (ICDD-JCPDS PDF-2 entry 01-072-130500-044-0673) and zinc sulphate hydroxide pentahydrate $Zn_4SO_4(OH)_6 \cdot 5H_2O$ (ICDD-JCPDS PDF-2 entry 01-072-130500-039-0688), which indicates the presence of a mixture of both compounds. The high intensity of ZHS doublet peak at 2θ angles $8.16°$ and $8.50°$ denoted as (a) in Fig. 1 corresponds to a very well-developed layered structure.

Diffractograms of samples S1, S2, and S3 are shown in the upper part of Fig. 1. Presence of both Fe_3O_4, and ZHS phases is clearly manifested. The intensities of the Fe_3O_4 lines grow with the increasing content of the magnetic component. On the other hand, the diffraction patterns for ZHS show remarkable alterations in the low diffraction angle region compared with the ZHS reference material. The intensity of the double line (a) close to $8°$ 2θ angles is significantly reduced. Moreover, the doublet peak almost disappears for sample S1, while the doublet (a) is broadened and merged into one peak denoted as (c) for samples S2 and S3. This can be attributed to a loss of stacking regularity in the layered mineral structure. On the contrary, the diffraction peak at $10.0°$ 2θ angle increases in height in the diffractogram, which confirms a decrease of the interlayer space due to the loss of intercalated water.

The morphologies of the Fe_3O_4 nanoparticles synthesized in the first step, the ZHS reference and the Fe_3O_4/ZHS nanocomposite are illustrated for sample S2 and shown in Fig. 3. A secondary electron image of Fe_3O_4 reveals close arrangement of highly uniform magnetic nanoparticles with diameters
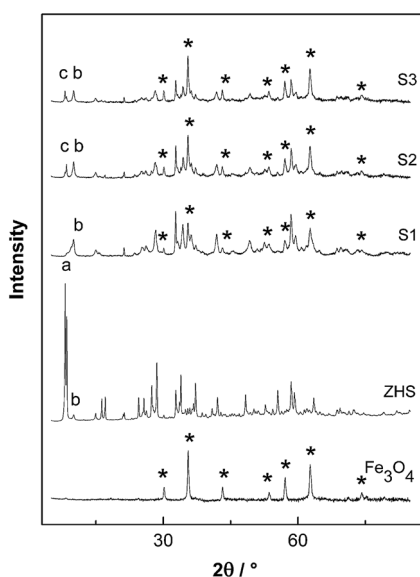

Fig. 2   XRD patterns of the reactants and products of the synthesis, when samples S1, S2 and S3 contain 50 mg, 100 mg and 150 mg of Fe_3O_4 for the synthesis.
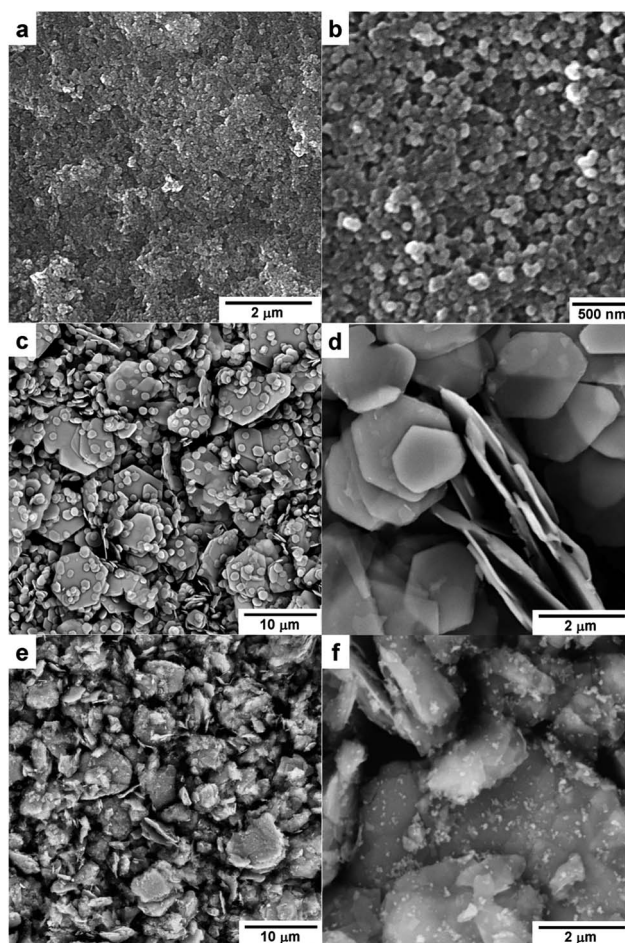

Fig. 3   SEM images of Fe_3O_4 nanoparticles (a and b), sample S2 (c and d) and sample S3 (e and f) at various magnifications.
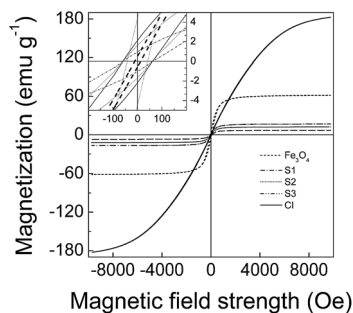
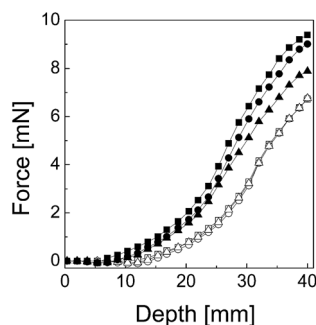Fig. 4   Magnetic properties of various samples.

Fig. 5   Dependence of the penetration force against depth for suspensions including 80 wt% of the bare CI particles (■, □), 80 wt% of the bare CI particles together with 1 wt% of sheet-like additive S3 (●, ○) and 80 wt% of the bare CI particles together with 5 wt% of sheet-like additive S3 (▲, △) in silicone oil for just prepared suspensions (open symbols) and measured after 7 days (solid symbols).

estimated in the range 50–100 nm (Fig. 3a and b). The reference ZHS material consists of sheet-like particles with evidently bimodal particle size distribution. The larger particles have a shape of hexagonal platelets with a diameter of about 10 μm, while the small particles having the same hexagonal shape are ten times smaller in diameter (Fig. 3c). Regardless of the size, the particles are very thin with a thickness less than 100 nm, as can be directly estimated from the lateral view of the particles shown in Fig. 3d. Moreover, the sheets in the upper right corner of the same figure are semitransparent in back-scattered (BSE) image mode even at an accelerated voltage of 10 kV. The micrographs confirm the well-developed structure of layered minerals, which is in accordance with the XRD analysis results.

The morphology of the Fe_3O_4/ZHS nanocomposite resembles the reference ZHS material in flatness, size, and diameter bimodality (Fig. 3e). On the other hand, a strong decrease of shape regularity is evident. The detailed micrograph in Fig. 3f allows an observation of the typical nanocomposite structure of the prepared materials in sample S2. Magnetic nanoparticles can be identified as bright points embedded within the ZHS two-dimensional matrix. Hence, each single platelet contains many uniformly-distributed magnetic nanoparticles, which cause a significant increase in the ZHS material disorder.

Although the particles' sheet-like morphology is somewhat disturbed, the nanoparticles impart magnetic properties to the hybrid composite sheets. The magnetic properties of bare CI

particles, Fe_3O_4 nanoparticles and synthesized hybrid composite particles with various amounts of Fe_3O_4 were measured by vibrating sample magnetometry (VSM). The recorded magnetization curves are shown in Fig. 4. The saturation magnetization of bare CI particles and Fe_3O_4 nanoparticles was 182.49 and 61.6 emu g⁻¹, respectively. In the case of synthesized Fe_3O_4/ZHS nanocomposites, the saturation magnetization increased from sample S1 (7.1 emu g⁻¹) over S2 (12.3 emu g⁻¹) to S3 (16.8 emu g⁻¹) with increasing Fe_3O_4 loading. Therefore, the sample S3, due to having the best magnetic properties, was used as an additive in MR suspensions.

3.2   Redispersibility of suspensions

In order to evaluate the redispersibility of suspensions consisting of bare CI particles as well as CI-based suspensions with various amounts of the sheet-like additive S3, dependence of the force applied to the suspension against the depth of the needle penetration was measured. As demonstrated in Fig. 5, a freshly-prepared suspension that includes bare CI particles exhibits nearly the same behaviour in comparison to other suspensions including various amounts of the sheet-like additive S3, however it should be mentioned that even the suspensions were freshly prepared, certain rich-phase of particles on the bottom of the flask was created prior to the measurement. On the other hand, a considerably different redispersibility of
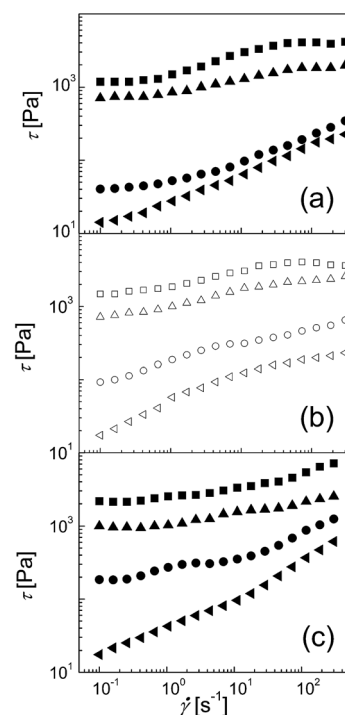

Fig. 6   Dependence of the shear stress, τ, on the shear rate, g, for suspensions of particles in silicone oil where are, (a) 80 wt% of bare CI particles, (b) 80 wt% of bare CI particles together with 1 wt% of sheet-like additive S3 and (c) 80 wt% of bare CI particles together with 5 wt% of sheet-like additive at various magnetic flux densities, B (mT): (◄, ◁) 0, (●, ○) 49, (▲, △) 171, (■, □) 279.
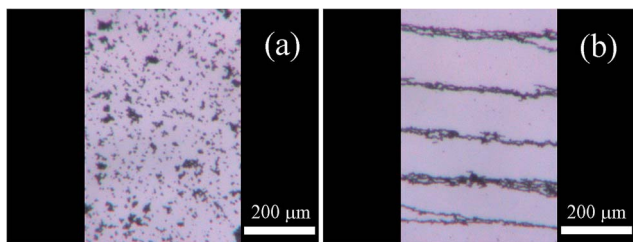
Fig. 7 Microscopic observation of the suspension containing 20 wt% of bare CI particles (a) in the absence of the magnetic field and (b) in the presence of the magnetic field of 120 mT.
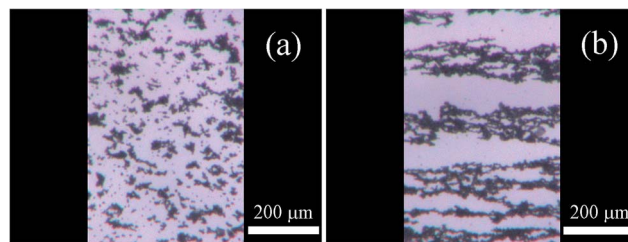

Fig. 9 Microscopic observation of the suspension containing 20 wt% of bare CI particles and corresponding amount of additive S3 (5 wt%) (a) in the absence of the magnetic field and (b) in the presence of the magnetic field of 120 mT.
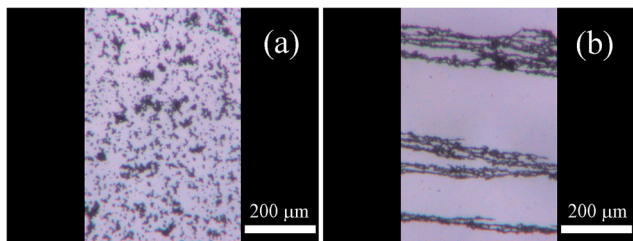

Fig. 8 Microscopic observation of the suspension containing 20 wt% of bare CI particles and corresponding amount of additive S3 (1 wt%) (a) in the absence of the magnetic field and (b) in the presence of the magnetic field of 120 mT.

Fig. 10 Dependence of the yield stress, τ_y, on the magnetic flux density, B, for particle silicone oil suspensions where ($\square$) 80 wt% of bare CI, ($\triangle$) 80 wt% of bare CI together with 1 wt% of sheet-like additive S3 and ($\bigcirc$) 80 wt% of bare CI together with 5 wt% of sheet-like additive S3.

those suspensions was observed after 7 days. The sample suspension including bare CI particles has visibly the worst redispersibility after the period of settling. The sample including 1 wt% of sheet-like additive S3 exhibits improved redispersibility, because the additive disturbs the usually good packing behaviour of the CI spherical particles, which results in lower applied force against the formed sediment. However, the considerably improved redispersibility was obtained for suspensions containing 5 wt% of sheet-like additive S3 when the presence of the additive significantly disturbs the packing properties of CI particles and thus contributes to enhanced redispersibility.

3.3 MR properties

The previous work published by Lopez-Lopez et al.[40] showed the significant increase in the yield stress of MR fluids when various amounts of magnetite nanoparticles (2, 10.8 or 21.6 vol%) were dispersed in the CI-based suspension. The explanation for this high increase in yield stress is that the nanoparticles in the system play a role of a surfactant when prevent the aggregation of the CI particles disturbing the remnant magnetization as well as the van der Waals interactions between them. Recent study published by Iglesias et al.[39] investigated the effect of smaller addition of the magnetite particles (3.1 or 7.9 vol%) on the MR performance. It was observed that small amount of magnetite provided an enhanced yield stress, due to the improved dipolar attraction between CI particles, while the higher amount of magnetite changed the behaviour to repulsive, due to the local inhomogeneity when the relatively high concentration of nanoparticles create chain-like structures along the applied
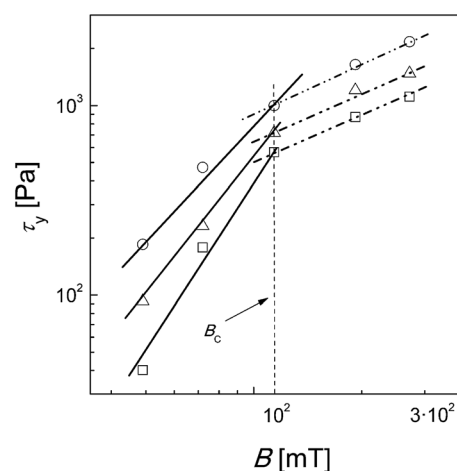
magnetic field and suppress the CI particle interactions. Also Chin et al.[41] was focused on the investigation of the effect of needle-like magnetic Cr_2O Co-γ-Fe_2O_3 additives on the CI-based suspension and they found out, that these particles exhibit not only enhanced sedimentation stability disturbing the packing perfection of bare CI ones, but also can facilitate the internal structure formation by various amount of the additive (1–10 wt%) most probably due to the irregular needle-like shape providing the better CI particle interactions.

Thus the MR behaviour of suspensions including 80 wt% of bare CI particles as well as the impact of the various amounts of the sheet-like additive S3 mixed into the 80 wt% of bare CI particle suspensions was investigated (Fig. 6). In the absence of an external magnetic field, all suspensions exhibit nearly New-tonian behaviour. Although, the amount of the particles in the system increases with additive content, the off-state behaviour is changed only slightly. However, a considerably different behaviour was observed after the application of the external magnetic field. As can be seen in Fig. 6a, the shear stress increases with increasing magnetic field strength for all suspension systems investigated. A small amount of sheet-like additive S3 (1 wt%) (Fig. 6b) increases MR performance

Table 1 Values of the slope for fitting of data with power-law relation $\tau_y \approx B^a$ at various magnetic flux densities

Sample	Suspension of bare CI particles	Suspension of bare CI particles with 1 wt% of samples S3	Suspension of bare CI particles with 5 wt% of samples S3
$B < 100$	2.2	2.12	2.05
$B > 100$	1.35	1.39	1.42

because the magnetic additive is able to provide more-developed internal structures created after the application of the external field in comparison to the bare CI-based suspensions. This behaviour is further promoted by an increased amount of the sheet-like additive S3 (5 wt%), and a nearly two times higher shear stress for this kind of suspension was obtained (Fig. 6c). Obviously, the sheet-like magnetic additive, due to its considerably different shape and mostly due to the micrometer particle size, contributes to better interparticle interactions and thus can improve the MR performance and provide more-developed internal structures in comparison with those obtained from the solely spherical bare CI. Similar behaviour was recently observed by the Piao *et al.* by addition of PANI/Fe0 nanofiber magnetic filler to CI-based suspensions even at lower concentration 0.1 wt%.[42] Finally, these outstanding findings can be further investigated, due to its possible industrial interest.

In order to confirm the improved MR behaviour of the suspensions containing magnetic additive S3, the microscopical observation in the absence as well as in the presence of the magnetic field was performed. In the absence of the external magnetic field the particles are randomly dispersed in case of all prepared suspensions. However, as can be seen in the Fig. 7, after application of the external field the suspension of bare CI particles provides rather thin internal structures between magnetic plates, aligned in the external field direction. Nevertheless, only small addition (1 wt%) of the magnetic additive S3 (Fig. 8) provides improved connection between the CI particles and internal structures are substantially developed. In this case, it can be also seen, that the internal structures are branched, providing the higher rigidity of the internal structures, due to presence of magnetic additive S3 and thus better interparticle interactions between CI. On the other hand, the higher amount (5 wt%) of the additive S3 (Fig. 9) present in the system considerably enhanced interparticle interactions and contributed to enhanced development of the internal structures. As can be seen highly branched internal structures are created perpendicularly to the magnetic plates assuring the improved MR performance. The considerably branched internal structures created upon external magnetic field, provide suspensions with better MR performance than those obtained for the suspensions containing only of bare CI particles, whose create single and not sufficiently branched internal structures, confirming the previous results from steady shear rheometry under external magnetic field.

The representative suspension property reflecting the stiffness of the internal structures is yield stress, τ_y. In this case the yield stress was evaluated using the Bingham model also employed by other groups[39,43] and evaluated as a function of magnetic flux density, B, using the power law relation $\tau_y \approx B^a$,

when the parameter a is a slope (Fig. 10). As it can be seen, at low magnetic flux densities below 100 mT, the slope differs due to the various compositions of the suspensions. A suspension without an additive has the steepest slope (2.2), and with increasing amount of the sheet-like additive S3 the slope slightly decreases to the value of 2 (Table 1) confirming the dipole model prediction for well-developed internal structures.[44] Furthermore, at high magnetic flux densities above 100 mT, the slopes are nearly the same for all measured suspensions (Table 1), and the values of the slope for all suspensions reach approximately 1.5 (dash double-dotted line), confirming the typical magnetization saturation behaviour.[30,45] In fact, the suspensions including sheet-like additives, exhibit two-times higher yield stresses in comparison to bare CI ones, while the off-state values sustain the same level. Such behaviour is mainly caused by the better dispersibility of the suspensions with additives and by the fact that these sheet-like magnetic particles can enhance the interparticle magnetostatic forces promoting better internal structure development and subsequently higher yield stresses. Finally, it can be seen that the amount of the additive has a negligible impact on the critical value of the magnetic flux density, B_c, above which the magnetic dipoles of the particles present in the suspensions can be locally saturated.[45]

4. Conclusion

This article presents the facile preparation of Fe_3O_4/ZHS hybrid composite sheets utilizing microwave-assisted synthesis. The preparation of a unique hybrid composite material was confirmed by X-ray diffraction, scanning electron microscopy, and vibrating sample magnetometry. The hybrid composite S3 with the highest magnetic properties was utilized as an additive to MR suspensions. In this case, the redispersibility properties of the suspensions increase with an increasing amount of magnetic additive, because the sheet-like additive disturbs the packing perfection of bare CI particles thus impeding their agglomeration. Finally, the suspension including 5 wt% of the sheet-like additive exhibits a nearly two times higher MR effect in comparison to those including only bare CI particles, due to their unique sheet-like shape, magnetic nature and micro-scale size. Therefore, it can be stated that even a small addition of the sheet-like particles can considerably improve the overall performance of MR suspensions.

Acknowledgements

References

1 G. Bossis, S. Lacis, A. Meunier and O. Volkova, *J. Magn. Magn. Matter.*, 2002, **252**, 224.
2 D. J. Klingenberg, J. C. Ulicny and M. A. Golden, *J. Rheol.*, 2007, **51**, 883.
3 A. J. F. Bombard, M. Knobel and M. R. Alcantara, *Int. J. Mod. Phys. B*, 2007, **21**, 4858.
4 B. J. Park, F. F. Fang and H. J. Choi, *Soft Matter*, 2010, **6**, 5246.
5 J. de Vicente, D. J. Klingenberg and R. Hidalgo-Alvarez, *Soft Matter*, 2011, **7**, 370.
6 W. L. Zhang and H. J. Choi, *J. Appl. Phys.*, 2014, **115**, 17B508.
7 Y. D. Liu and H. J. Choi, *J. Appl. Phys.*, 2014, **115**, 17B529.
8 G. R. Iglesias, M. T. Lopez-Lopez, A. V. Delgado and J. D. G. Duran, *Rev. Sci. Instrum.*, 2011, **82**, 073906.
9 A. J. F. Bombard and J. V. R. Teodoro, *Int. J. Mod. Phys. B*, 2011, **25**, 943.
10 M. Sedlacik and V. Pavlinek, *RSC Adv.*, 2014, **4**, 58377.
11 Q. C. Gong, J. K. Wu, X. L. Gong, Y. C. Fan and H. S. Xia, *RSC Adv.*, 2013, **3**, 3241.
12 J. L. Viota, F. Gonzales-Caballero, J. D. G. Duran and A. V. Delgado, *J. Colloid Interface Sci.*, 2007, **309**, 135.
13 M. Mrlik, M. Sedlacik, V. Pavlinek, P. Bazant, P. Saha, P. Svrcinova and P. Filip, *J. Appl. Polym. Sci.*, 2013, **128**, 2977.
14 K. von Pfeil, M. D. Graham, D. J. Klingenberg and J. F. Morris, *Phys. Rev. Lett.*, 2002, **88**, 188301.
15 D. Case, B. Taheri and E. Richer, *IEEE ASME Trans. Mechatron.*, 2013, **18**, 96.
16 B. Gonenc and H. Gurocak, *Mechatronics*, 2012, **22**, 1161.
17 D. M. Wang, Y. F. Hou and Z. Z. Tian, *Smart Mater. Struct.*, 2013, **22**, 025019.
18 E. Kostamo, M. Focchi, E. Guglielmino, J. Kostamo, C. Semini, J. Buchli, M. Pietola and D. Caldwell, *J. Mech. Des.*, 2014, **136**, 021003.
19 M. Sedlacik, R. Moucka, Z. Kozakova, N. E. Kazantseva, V. Pavlinek, I. Kuritka, O. Kaman and P. Peer, *J. Magn. Magn. Mater.*, 2013, **326**, 7.
20 Y. D. Liu, F. F. Fang and H. J. Choi, *Colloid Polym. Sci.*, 2011, **289**, 1295.
21 M. Sedlacik, V. Pavlinek, M. Lehocky, A. Mracek, O. Grulich, P. Svrcinova, P. Filip and A. Vesel, *Colloids Surf., A*, 2011, **387**, 99.
22 X. Z. Zhang, W. H. Li and X. L. Gong, *Smart Mater. Struct.*, 2010, **19**, 125012.
23 J. L. Viota, J. de Vicente, J. D. G. Duran and A. V. Delgado, *J. Colloid Interface Sci.*, 2005, **284**, 527.
24 M. Sedlacik, V. Pavlinek, P. Saha, P. Svrcinova, P. Filip and J. Stejskal, *Smart Mater. Struct.*, 2010, **19**, 115008.
25 J. H. Park, B. D. Chin and O. O. Park, *J. Colloid Interface Sci.*, 2001, **240**, 349.
26 F. F. Fang, H. J. Choi and W. S. Choi, *Colloid Polym. Sci.*, 2010, **288**, 359.
27 F. F. Fang, H. J. Choi and Y. Seo, *ACS Appl. Mater. Interfaces*, 2010, **2**, 54.
28 F. F. Fang and H. J. Choi, *Colloid Polym. Sci.*, 2010, **288**, 79.
29 M. Machovsky, M. Mrlik, I. Kuritka, V. Pavlinek and V. Babayan, *RSC Adv.*, 2014, **4**, 996.
30 F. F. Fang, Y. D. Liu, H. J. Choi and Y. Seo, *ACS Appl. Mater. Interfaces*, 2011, **3**, 3487.
31 M. Mrlik, M. Ilcikova, V. Pavlinek, J. Mosnacek, P. Peer and P. Filip, *J. Colloid Interface Sci.*, 2013, **396**, 146.
32 M. Mrlik, M. Ilcikova, V. Pavlinek, J. Mosnacek, P. Peer and P. Filip, *Colloid Polym. Sci.*, 2014, **292**, 2137–2143.
33 J. L. Viota, A. V. Delgado, J. L. Arias and J. D. G. Duran, *J. Colloid Interface Sci.*, 2008, **324**, 199.
34 M. Sedlacik, V. Pavlinek, R. Vyroubal, P. Peer and P. Filip, *Smart Mater. Struct.*, 2013, **22**, 035011.
35 X. M. Quan, Y. D. Liu, W. S. Ahn and H. J. Choi, *IEEE Trans. Magn.*, 2013, **49**, 3410.
36 W. L. Zhang, S. D. Kim and H. J. Choi, *IEEE Trans. Magn.*, 2014, **50**, 2500804.
37 Z. Kozakova, P. Bazant, M. Machovsky, V. Babayan and I. Kuritka, *Acta Phys. Pol., A*, 2010, **118**, 948.
38 M. Machovsky, I. Kuritka, J. Sedlak and M. Pastorek, *Mater. Res. Bull.*, 2013, **48**, 4002.
39 G. R. Iglesias, M. T. Lopez-Lopez, J. D. G. Duran, F. Gonzales-Caballero and A. V. Delgado, *J. Colloid Interface Sci.*, 2012, **377**, 153.
40 M. T. Lopez-Lopez, P. Kuzhir, S. Lacis, G. Bossis, F. Gonzales-Caballero and J. D. G. Duran, *J. Phys.: Condens. Matter*, 2006, **18**, S2803.
41 B. D. Chin, J. H. Park, M. H. Kwon and O. O. Park, *Rheol. Acta*, 2001, **40**, 211.
42 S. H. Piao, M. Bhaumik, A. Maity and H. J. Choi, *J. Mater. Chem. C*, 2015, DOI: 10.1039/c4tc02491e.
43 J. de Vicente, J. D. G. Durán, A. V. Delgado, F. Gonzales-Caballero and G. Bossis, *Int. J. Mod. Phys. B*, 2002, **16**, 2576.
44 J. M. Ginder and L. C. Davis, *Appl. Phys. Lett.*, 1994, **65**, 3410.
45 J. M. Ginder, L. C. Davis and L. D. Elie, *Int. J. Mod. Phys. B*, 1996, **10**, 3293.